Multiple attenuation with a modified parabolic Radon transform

B. Ursin*, B. Abbad, NTNU, Trondheim, Norway,
M. J. Porsani, UFBA, Salvador, Brazil.

This paper was prepared for presentation during the 11th International Congress of the Brazilian Geophysical Society held in Salvador, Brazil, August 24-28, 2009.

Abstract

We present a fast and efficient frequency-domain implementation of a modified parabolic Radon transform (modified PRT) based on a singular value decomposition with applications to multiple removal. With a change of variable, the problem is transformed into a complex linear system involving a single operator after merging the curvature-frequency parameters into a new variable. A complex singular value decomposition (SVD) can be applied to this operator and the forward modified parabolic Radon transform is computed for all frequency components within the signal bandwidth by means of complex back-substitution only.

The standard PRT can be obtained by interpolation in the modified transform domain. The method is also able to resolve the multiple energy from the primaries when they interfere in a small time interval and resists well to AVO effects in the data. The proposed modified PRT was successfully applied to a deep-water seismic line at the Gulf of Mexico to attenuate water-bottom multiples and subsequent peg-legs originating from multiple paths in the water column.

The modified parabolic Radon transform

The inverse parabolic Radon transform is defined as a decomposition of seismic data in the curvature-intercept time domain using a set of curvature values $q_k, k=1,N_q$. For discrete seismic data $D(x_n,t)$ recorded at offset x_n and time t, this is defined by a sum along parabolic paths in the $q-\tau$ domain (Hampson, 1986)

$$D(x_n,t)=\sum_{j=1}^{N_q} M\left(q_j,\tau=t-q_j x_n^2\right) \quad n=1,\cdots,N_x \qquad (1)$$

where $M(q,\tau)$ represents the parabolic Radon transform at curvature q and intercept time τ, and N_q being the number of Radon curvatures while N_x denotes the number of seismic traces. Using the linearity property of the Fourier transform, equation (1) can be expressed in the frequency domain as

$$d(x_n,f)=\sum_{j=1}^{N_q} m(q_j,f)e^{2\pi i f q_j x_n^2}. \qquad (2)$$

Equation (2) is a complex linear system for a given frequency f. In matrix notation, this can be written as

$$\mathbf{d}(f)=\mathbf{L}(f)\mathbf{m}(f), \qquad (3)$$

where $\mathbf{d}(f)$ and $\mathbf{m}(f)$ are frequency-dependent vectors. The elements of the matrix $\mathbf{L}(f)$ have the form

$$L_{kj}(f)=e^{2\pi i f q_j x_k^2}\ k=1,\cdots,N_x;\ j=1,\cdots,N_q. \qquad (4)$$

The above formulation of the PRT requires solving the inverse problem in (3) for each frequency component in the signal bandwidth to compute the transform because the complex operator $\mathbf{L}(f)$ is frequency-dependent leading to a different matrix for each spectral component. To remove the frequency-dependence in the transform operator $\mathbf{L}(f)$, we introduce a new variable $\lambda=qf$ with unit m^{-2}. Writing (2) in terms of the variable λ leads to the following system of complex equations

$$d(x_n,f)=\sum_{j=1}^{N_q} m(\lambda_j,f)e^{2\pi i \lambda_j x_n^2}. \qquad (5)$$

This can be written in a more compact form as

$$\mathbf{d}(f)=\mathbf{L}(\lambda)\mathbf{m}(f), \qquad (6)$$

where the $N_x\times N_\lambda$ complex matrix $\mathbf{L}(\lambda)$ defined as

$$L_{kj}(\lambda)=e^{2\pi i \lambda_j x_k^2}\ k=1,\cdots,N_x;\ j=1,\cdots,N_q \qquad (7)$$

Equations (5) or (6) correspond to a modified PRT which can be computed much faster than the standard PRT because the inverse of the matrix $\mathbf{L}(\lambda)$ has to be computed only once, given a data acquisition geometry $[x_n, n=1,\cdots,N_x]$ and a chosen discretization $[\lambda_j, j=1,\cdots,N_\lambda]$. The standard PRT in the frequency domain, $m(q,f)$, can be obtained by interpolation in the modified PRT domain.

The minimum-norm solution

In a high-resolution modified PRT, we choose the number of λ-values, $N_\lambda > N_x$. Then the problem is under-determined and we choose the minimum-norm solution which can be written as

$$\mathbf{m_{MN}}(f)=\mathbf{L}^{\mathbf{H}}(\lambda)\left[\mathbf{L}(\lambda)\mathbf{L}^{\mathbf{H}}(\lambda)\right]^{-1}\mathbf{d}(f). \qquad (8)$$

We use the SVD decomposition for the operator $\mathbf{L}(\lambda)$

$$\mathbf{L}(\lambda) = \mathbf{U}\left[\Sigma \quad 0\right]\mathbf{V}^{\mathbf{H}}, \tag{9}$$

where $\Sigma = diag\left[\sigma_1, \sigma_2, \cdots, \sigma_{N_x}\right]$ with $\sigma_1 \geq \sigma_2 \geq \cdots \geq \sigma_{N_x} \geq 0$, to obtain a stable estimate

$$\mathbf{m_{MN}}(f) = \mathbf{V}\begin{bmatrix}\Sigma^{\dagger} \\ \mathbf{0}\end{bmatrix}\mathbf{U}^{\mathbf{H}}\mathbf{d}(f), \tag{10}$$

where $\Sigma^{\dagger}$ is the pseudo-inverse of Σ with components

$$\sigma_k^{\dagger} = \begin{cases}\sigma_k^{-1} & \text{if } \sigma_k \geq \varepsilon \\ 0 & \text{if } \sigma_k < \varepsilon\end{cases}, k = 1, \cdots, N_{\lambda}. \tag{11}$$

The transformations $\tilde{\mathbf{m}}_{\mathbf{MN}}(f) = \mathbf{V}^{\mathbf{H}}\mathbf{m}_{\mathbf{MN}}(f)$ and $\tilde{\mathbf{d}}(f) = \mathbf{U}^{\mathbf{H}}\mathbf{d}(f)$ give

$$\tilde{\mathbf{m}}_{\mathbf{MN},k}(f) = \begin{cases}\sigma_k^{\dagger}\tilde{\mathbf{d}}_k(f) & k = 1, \cdots, N_x \\ 0 & k = N_x + 1, \cdots, N_{\lambda}\end{cases}. \tag{12}$$

We see that the last components of $\tilde{\mathbf{m}}_{\mathbf{MN}}$ are zero, corresponding to the minimum-norm properties of the solution $\mathbf{m_{MN}}$.

Multiple attenuation

We may attenuate multiple reflections in the $\lambda - f$ domain by partly correcting the seismic data for normal moveout effects such that the primary reflections appear with less moveout than multiple reflections. The main assumption on seismic data input to the transform is that residual moveouts of both primary and multiple reflections have parabolic behavior as a function of offset (Hampson, 1986). The data are transformed to the $\lambda - f$ domain using an inverse operator

$$\hat{\mathbf{m}}(f) = \mathbf{L}^{\dagger}(\lambda)\mathbf{d}(f), \tag{13}$$

defined in equation (10). An estimate of the primary reflections are obtained by filtering the data $\hat{\mathbf{m}}_{\mathbf{P}}(f) = \mathbf{F}(\lambda, f)\hat{\mathbf{m}}(f)$ where the filter is

$$\mathbf{F}(\lambda, f) = \begin{cases}1 & \text{for } \lambda \leq q_0 f \\ 0 & \text{for } \lambda > q_0 f\end{cases}, \tag{14}$$

where q_0 is a curvature parameter that separates primaries and multiples. The primary reflections are then obtained by transforming back to the $x - f$ domain

$$\mathbf{d_P}(f) = \mathbf{L}(\lambda)\mathbf{F}(\lambda, f)\mathbf{L}^{\dagger}(\lambda)\mathbf{d}(f) = \mathbf{G}(\lambda, f)\mathbf{d}(f). \tag{15}$$

The matrix $\mathbf{G}(\lambda, f) = \mathbf{L}(\lambda)\mathbf{F}(\lambda, f)\mathbf{L}^{\dagger}(\lambda)$ has a dimension $N_x \times N_x$. It behaves as a filter applied to seismic data in the frequency-offset domain to remove multiples directly from the data. The multiples can be also estimated using the following relationship

$$\mathbf{d_M}(f) = \left[\mathbf{I}_{N_x \times N_x} - \mathbf{G}(\lambda, f)\right]\mathbf{d}(f). \tag{16}$$

where $\mathbf{I}_{N_x \times N_x}$ is the identity matrix. For a given frequency, the operator $\mathbf{G}$ depends only on the data acquisition parameters, our choice of parameters in the λ-domain, and the choice of parameters for the pseudo-inverse.

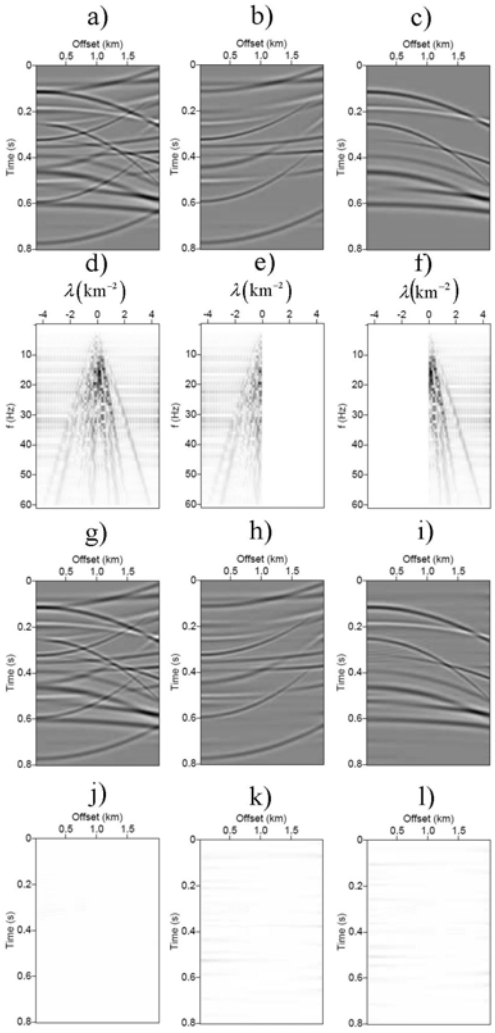

Figure 1. The modified PRT for the gather with AVO effects included along the events.

Examples

A complex synthetic example that consists of a large number of events (20 parabolas) interfering in a narrow time window is illustrated in Figure 1a. This model contains 12 primaries with negative curvatures (Figure 1b) and 8 multiples with positive curvatures (Figure 1c). We included AVO effects along the parabolic moveouts according to the function

$$A(y) = a_0 + a_1 y + a_2 y^2;\ y = \frac{|x|}{x_{\max}}, \tag{17}$$

where y is the normalized offset, $a_0, a_1,$ and a_2 are real coefficients. The modified PRT is implemented using a fine sampling leading to an under-determined problem to obtain a dense Radon space (250-λ traces for 100 seismic traces) which makes demultiple more efficient. The curvature was scanned for in the range $\left[-0.30s - +0.30s\right]$ which gives a λ – parameter varying in

the interval $[-4.5\ km^{-2} - +4.5\ km^{-2}]$. We used symmetric moveout range for scan to allow the mapping of all the events in the gather.

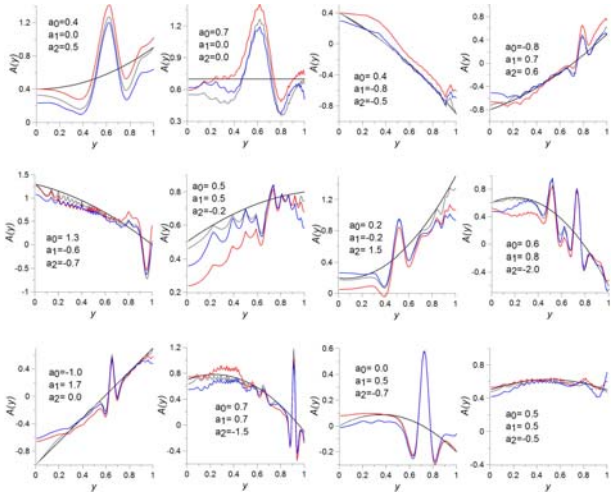

Figure 2. Theoretical and inverted AVO curves in the example of Figure 1 for the 12 primary events using both the modified PRT and the IRLS methods.

We used the minimum-norm solution which converts the problem into a hermitian inverse problem of dimension $N_x \times N_x$ as provided by equation (8). The eigenvalue decomposition of the minimum-norm operator gives a condition number equal to 7.34×10^4 for $N_\lambda = 250$. To account for this, the inverse operator was stabilized using a truncation limit at $\varepsilon = 10^{-3}$ which reduces the numerical rank of $\mathbf{L}(\lambda)$ by ignoring small singular values.

The mapping of the whole gather in Figures 1a in the $\lambda - f$ domain is shown in Figures 1d. Primary and multiple energy are mapped in distinct areas of the $\lambda - f$ domain. Each event with parabolic moveout in the time-offset domain is transformed along a radial line in the $\lambda - f$ domain passing through the origin and characterized by the respective event curvature as the slope value with a frequency extent shaping the event wavelet bandwidth (spectrum).

According to this, events with positive curvatures $q > 0$ are mapped into the positive $\lambda -$ space while negative $\lambda -$ space contains events with $q \le 0$. Figures 1e and 1f illustrate how the events in the gathers of Figures 1b and 1c are transformed in the modified PRT domain. Since primaries have negative curvatures in the example, a mute zone was established at $\lambda = 0$ to separate primaries from multiples. The reconstructed gathers after inverse transform are shown in Figures 1g, 1h, and 1i, they show the events in the original gather with their true curvature and amplitude characteristics.

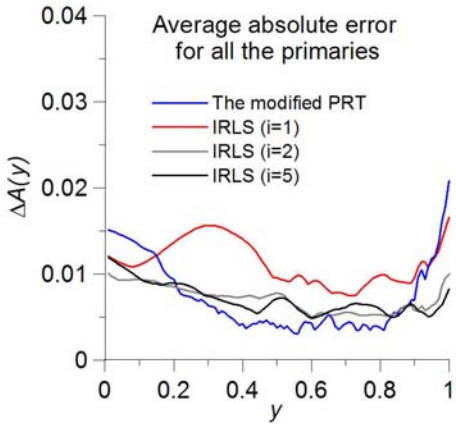

Figure 3. Average absolute error on the AVO inverted curves in the example of Figure 1 over the 12 primary events using both the modified PRT and the IRLS methods.

The reconstruction errors for the three gathers are depicted in Figures 1j, 1k, and 1l. This error is very small for the whole gather and is mainly due to the use of truncation in estimating the pseudo-inverse of $\mathbf{L}(\lambda)$. All PRT methods suffer such residual errors after reconstruction due to the ill-conditioning of the inverse problem. The residual errors from separating primaries and multiples show inverse signs on both gathers occurring mainly along the axis $\lambda = 0$ thus generating horizontal low-amplitude artifacts in the filtered gathers.

The amplitude effects on the 12 primary events (in Figure 1b) are plotted in Figure 2 (curve in black). These show significant amplitude changes with normalized offset and several zero-crossings can be observed. The coefficients (a_0, a_1, a_2) are given on each plot for the respective event.

The event interference between primaries and multiples and between primaries alone leads to amplitude distortion on individual events in the gather. Thus, the amplitudes of the events being interfered add to each other within the crossing area, hence altering the AVO curve and making the amplitude inversion inaccurate. The grey curves in Figure 2 show the practical amplitude functions for each event of the primaries that accounts for the interference with the other primaries. Outside the interference zone, the theoretical and practical amplitude curves are equal.

The recovered amplitude functions of the primaries after demultiple are also drawn in Figure 2 (curves in blue). Schonewille and Zwartjes (2001) proposed a sparseness-constrained frequency-domain algorithm resisting well to AVO effects, where the weighting matrix is obtained by averaging the model within the signal bandwidth at the previous iteration to constrain the solution at the current iteration. Their method can be implemented using the iteratively reweighted least-squares (IRLS) algorithm combined with a complex version of the LSQR solver. Both algorithms give comparable results, but the modified PRT algorithm has the advantage to be extremely fast.

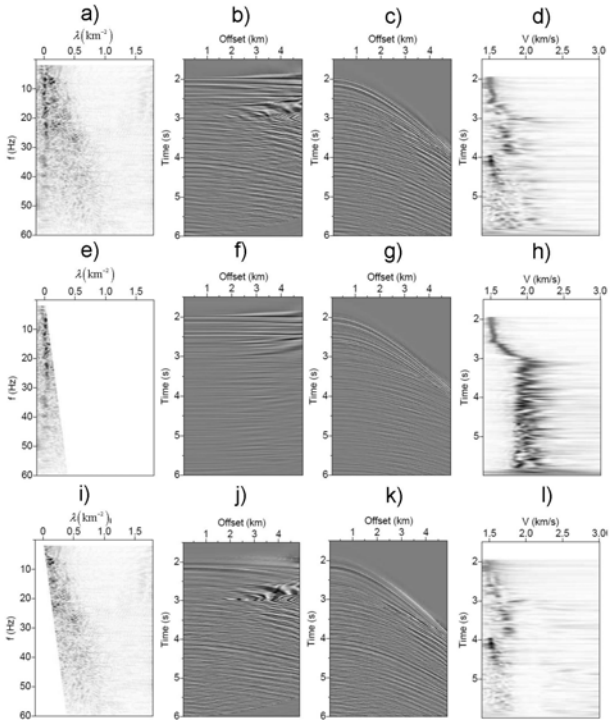

Figure 4. The modified PRT for a real data gather from the Gulf of Mexico.

The amplitude curves recovered from applying the IRLS method are shown by the red curve in Figure 2 for the 12 events after a single iteration. From the curves, we observe that both methods provide a good reconstruction of the practical amplitude functions along the primaries at most offsets despite the strong interference in the treated example. The recovered amplitudes are very accurate at most offsets. At medium offsets, the suggested approach allows for more accurate conservation of the AVO curve than does the IRLS method. At near offsets, the IRLS method has generally smaller amplitude errors but the error is larger than the modified PRT for some primaries (events 6 and 7 for instance). The same observation can be made at very far offsets where the IRLS method performs slightly better. The proposed method proves higher accuracy in amplitude recovery than the IRLS approach at most offsets. This observation is further confirmed on Figure 3 which depicts the average absolute amplitude error for the 12 events in Figure 1b. The superiority in performance of our approach (blue curve) is again demonstrated except at the extreme offsets in the data. The grey and black curves in Figure 2 show the absolute errors of the AVO function using 2 and 5 iterations in the IRLS approach, respectively. With further iterations in the IRLS method, increased accuracy is achieved at most offsets. However, a loss of accuracy can also be observed at intermediate offset ranges when comparing results after 2 and 5 iterations. There is a significant reduction of the errors associated with most offsets than the first iteration (red curve) but these errors still larger than the modified PRT errors at most offsets which has the added advantage to be very fast.

The modified PRT method was also tested on a marine seismic line from the Golf of Mexico characterized by a deep sea-bottom with important amplitude variations with offset and water-bottom multiples. Figure 4c shows a gather from the survey and illustrates the strong interference in the area and the large number of events recorded. Nonhyperbolic velocity analysis was performed on the data to generate post-NMO data to be input for the modified PRT algorithm. A velocity spectrum computed using the semblance coefficient is given in Figure 4d. The decrease of stacking velocities after 4*s* is an obvious indicator to the presence of water-bottom multiple reflections and peg-legs originating from the thin layers just below the sea-bed. Figure 4b shows the gather after applying nonhyperbolic NMO corrections with parameters derived from velocity analysis. The primary energy corrected with the exact moveout parameters (NMO velocity and effective anellipticity) is well flattened in the full offset range, whereas multiple energy has positive residual moveouts that can be well approximated using parabolic curves as observed in the lower part of the gather after 4*s*.

To accelerate computations, the modified PRT was applied in the time range $[1.5s - 6.0s]$, thus concerning only the area below sea-bottom where events are recorded. The moveouts were scanned for in the time range $[-0.05s - +0.70s]$ at the maximum offset in the gather. To implement the transform, the maximum signal frequency was set to $60Hz$, which gives a $\lambda-$range in the interval $\left[-0.127km^{-2} - 1.79km^{-2}\right]$. To conserve the whole amplitude information in the primaries, we used a filter cut-off at a positive curvature value $q_0 = 4.26\times10^{-3} s/km^2$, thus corresponding to a radial mute zone in the $\lambda - f$ domain defined by the equation $\lambda = 4.26\times 10^{-3} f$. The respective $\lambda - f$ domains for the different wave modes are given in Figures 4e and 4i for the primary and the multiple modes, respectively, where the separation between the trends is obvious. The data gathers corresponding to these domains are computed through equation (6) and are illustrated in Figures 4f and 4j. Inverse nonhyperbolic moveout corrections help in reconstructing the original gathers filtered into primary (Figure 4g) and multiple (Figure 4k) modes. These gathers show that multiples are concentrated in the lower part of the gather due to multiple paths in the water-column and peg-legs in subsequent thin layers below the sea-bed. The velocity spectra for the filtered primaries and multiples are respectively depicted in Figures4h and 4l. After demultiple, significant primary energy is recovered after 4 s and can be clearly recognized in the primary gather (Figure 4g) and also in the velocity spectrum (Figure 4h).

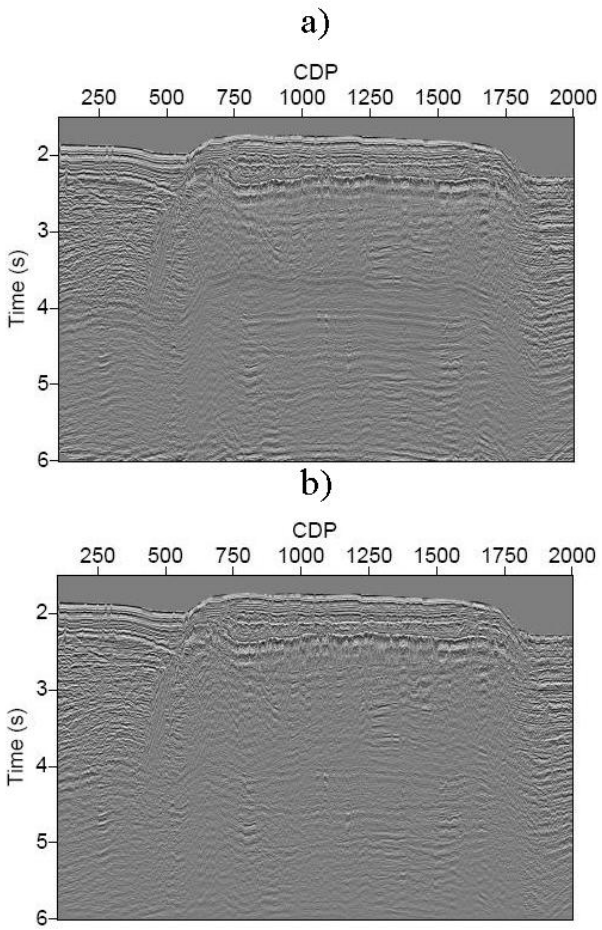

Figure 5. Processing results of the Gulf of Mexico data set. a) Stacked section without demultiple. b) Stack obtained with multiple removal using the modified PRT.

Figure 5a shows the stack obtained from nonhyperbolic velocity analysis without any demultiple. The stack illustrates the main features of the area mainly a salt body. The lower part of the stack is dominated by multiple reflections after 3.5*s*. The modified PRT is applied to this seismic line in the aim to attenuate water-bottom multiples and subsequent peg-leg reflections. The obtained stack is depicted in Figure 5b and demonstrates how the algorithm allowed for efficient demultiple. The multiple energy in the section of Figure 5a was mostly removed particularly the reflected waves with multiple paths in the water layer located in time between 3.5 s and 4.0 s. The multiple energy located in later times is due to the peg-leg multiples and was successfully attenuated.

Conclusions

A fast implementation of a modified parabolic Radon transform is proposed in this paper. The transform is linked to the standard PRT by means of interpolation. The new method shows high performance in conserving accurate AVO effects after the demultiple process which has several practical benefits. The method allows also for time savings especially in large data sets such those encountered in deep marine explorations or in 3D acquisitions. The modified PRT method satisfies exactly the sampling conditions and offers a wider $q-$range at all frequencies than does the standard PRT.

Acknowledgements

This project received financial support from the Norwegian University of Science and Technology (NTNU), PetroMax, the Federal University of Bahia (UFBA), CNPq, StatoilHydro ASA through the VISTA project, and the Norwegian Research Council through the ROSE project. BA wishes to thank Eric Duveneck for early support on this project and Martin Landro for fruitful discussion.

References

Hampson, D., 1986, Inverse velocity stacking for multiple elimination, Journal of the Canadian Society of Exploration Geophysicists, **22**, 44-55.

Hugonnet, P., and G. Canadas, 1995, Aliasing in the parabolic Radon transform: The 65th Annual International Meeting, SEG, Expanded Abstracts, 1366-1369.

Schonewille, M.A., and A. J. W. Duijndam, 2001, Parabolic Radon transform, sampling and efficiency: Geophysics, **66**, 667-678.

Schonewille, M.A., and P. Zwartjes, 2001, High-resolution transforms and amplitude preservation: The 72th Annual International Meeting, Society of Exploration Geophysicists, Expanded Abstracts, 2066-2069.